XRD and AFM characterization of Diarun-MgO-Averaplus fabricated Nanoparticles using precipitation method

M. Udayendiran[1],A. Christy Ferdinand[*,2], T. Kasthury[2]

[1]Research Scholar, PG & Research Department of Physics, Periyar Government Arts College, Cuddalore - 607001, Tamil Nadu, India.

[*,2]PG & Research Department of Physics, Periyar Government Arts College, Cuddalore - 607001, Tamil Nadu, India.

Corresponding Author: christyferdinand2@gmail.com (A.Christy Ferdinand)

Abstract

The importance of nanomaterials to the pharmaceutical industry is evident - over 90% of pharmaceutical products contain a drug in nano form. However, the nanomaterial phenomena of drug compounds are poorly understood. An increased understanding of these processes may allow a greater degree of control over the outcomes, such as morphology, purity, or stability. In these studies, we have applied Atomic Force Microscopy (AFM) to the in situ investigations of drug crystal growth. This study comprehensively investigates the physicochemical properties of Diarun, MgO, AveraPlus nanomaterials synthesized via three different chemical precipitation method at three annealing temperatures. X-ray diffraction (XRD) analysis reveals the crystalline structure and phase composition, highlighting changes in crystalline and phase transitions with varying annealing temperatures. The annealing process was employed to enhance the crystallinity and interfacial interactions between the constituents, thereby improving the overall thermal stability and performance of the nanocomposites. A comprehensive characterization was conducted using X-ray diffraction (XRD), atomic force microscopy (AFM) offered surface morphology and topography details. Particle size analysis enabled the determination of size distribution. This multi-technique approach provides a thorough understanding of the structural, chemical, optical, morphological, and size-related properties of Diarun + MgO nanocomposites, crucial for their potential applications.

Keywords: Diarun, Averaplus, Magnesium Oxide, chemical synthesis, AFM,XRD

1. Introduction

In recent years, magnetic nanocomposites have emerged as promising candidates for targeted drug delivery, offering precise control over drug release and localization [1]. This is attributed to their ability to be manipulated by external magnetic fields, directing them to specific sites within the body [2]. One such nanocomposite of interest is the Diarun ,MgO , Avera Plus blend in different ratio, which combines the therapeutic properties of Diarun, a polyherbal formulation known for its antidiabetic, antioxidant, and hypolipidemic effects [3], with the magnetic properties of MgO nanoparticles and the bioactive components of AveraPlus, Diarun, a polymer known for its excellent mechanical properties and chemical resistance, when combined with MgO, a widely studied metal oxide nanoparticle renowned for its high surface area and catalytic activity, and Avera Plus, a bioactive compound with potential medicinal applications, offers a synergistic platform for multifunctional nanocomposite development.The herbal ingredients within Diarun have demonstrated promising antidiabetic effects in experimental models [4] and have shown efficacy in improving glucose tolerance and lowering fasting blood glucose levels [5]. Additionally, magnesium, an essential mineral and abundant intracellular caution [6], plays a crucial role in enzymatic processes related to energy metabolism and glucose regulation [7]. Clinical studies have also highlighted the inverse relationship between serum magnesium levels and markers of inflammation [8], suggesting a potential role for magnesium in modulating inflammatory responses and insulin sensitivity [9].

The synthesis and characterization of Diarun-MgO-Avera Plus nanocomposites have been the subject of growing research interest, driven by the pursuit of tailored material properties for diverse applications. Previous studies have demonstrated the feasibility of incorporating these components into nanocomposite structures via various fabrication methods, including chemical precipitation, sol-gel, and melt blending techniques [10-12]. Additionally, the characterization of such nanocomposites has relied on a suite of analytical techniques, including X-ray diffraction (XRD) and Atomic force microscopy (AFM) to comprehensively elucidate their structural, optical, morphological, and surface properties [13-15,19].In this context, this study aims to systematically investigate the effects of annealing

temperature on the structural, optical, and morphological properties of Diarun-MgO-Avera Plus nanocomposites synthesized via chemical precipitation, Co-Precipitation methodand wet chemical method. By employing a multidimensional characterization approach encompassing XRD and AFM this research endeavors to provide insights into the structural evolution, phase transformations, chemical bonding, optical behavior, surface morphology, and particle size distribution of the nanocomposites at different annealing temperatures. Such insights are crucial for optimizing the fabrication process and tailoring the properties of Diarun-MgO-Avera Plus nanocomposites for applications ranging from biomedicine to catalysis and beyond.

By combining Diarun with MgO and Avera Plus in a nanocomposite formulation, there is potential for synergistic therapeutic effects, including targeted drug delivery and modulation of inflammatory pathways[16-18]. However, further investigation is needed to elucidate the specific mechanisms underlying the therapeutic potential of this nanocomposite blend.Through this introduction, we aim to highlight the multifaceted therapeutic potential of Diarun-MgO-Avera Plus nanocomposites, encompassing their targeted drug delivery capabilities and the synergistic effects of their constituent herbal ingredients and magnesium[20]. The referenced studies provide a robust foundation for understanding the therapeutic mechanisms and clinical implications of these nanocomposites in the context of diabetes management and inflammation modulation.

2. Materials and Methods

2.1. Materials used

The materials used in the synthesis include Avera Plus and Diarun, which were both purchased from (RumiHerbals, 99%),. In addition, the synthesis procedure made use of analytical-grade double-distilled water, sodium hydroxide (NaOH), and magnesium oxide MgO (Merck, 99%), were employed in the synthesis procedure.

2.2. Precipitation Method

Nanomaterial synthesis methods encompass a wide range of techniques tailored to produce nanoparticles, nanowires, nanotubes, and other nanostructures with precise control over

size, shape, and composition. These methods can be categorized into physical, chemical, and biological approaches, each offering unique advantages and challenges. Chemical synthesis methods, including Chemical precipitation, co precipitation synthesis, wet chemical method rely on chemical reactions to nucleate and grow nanoparticles from precursor materials in solution. These methods enable precise control over nanoparticle size, shape, and composition and are widely used in fields such as catalysis, sensing, and drug delivery.

Atomic Force Microscope Analysis

Sample A : 30% diarun + 70% MgO NPs at 200 ° C, 400 ° C, 600 ° C

Atomic force microscopic examination allows identifying the plot topographies representing the surface elevation and the structure of the surface. This technique refers to digital images that allow quantitative measurements of surface features, such as root mean square roughness (Rq), average roughness (Ra) and the analysis of images from different perspectives, including 3D simulation.Figure-1, Figure-2 and Figure-3, illustrates the three dimensional AFM images and granularity distribution of the sample 30% diarun + 70% MgO NPs synthesized by the chemical precipitation methods at different annealing temperatures. It is important to note that the mean values were obtained and showed a statistical variance, depending on the location of the measurements performed on the samples. The average grain size for the sample 30% diarun + 70% MgO NPs was 17.162 nm, as show in Table-1.

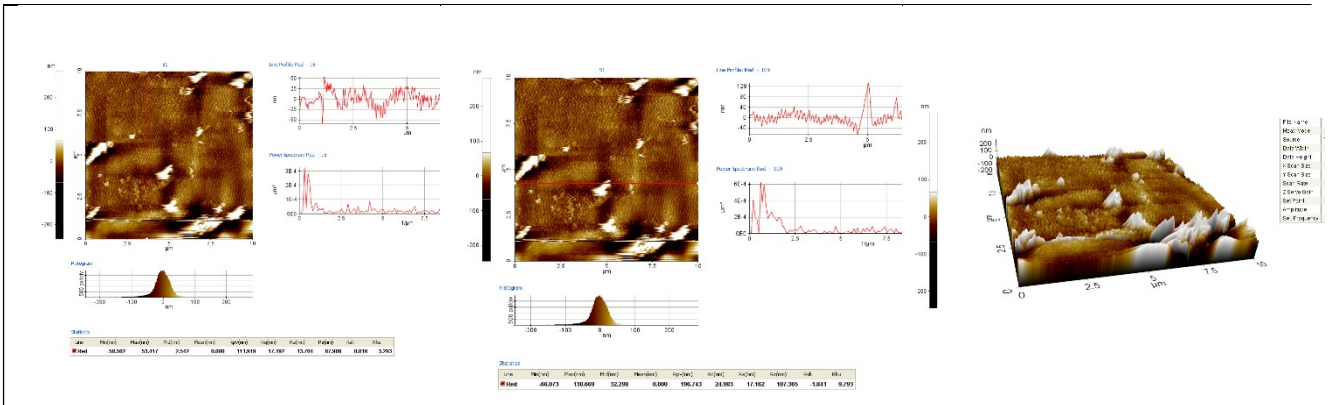

(a)	(b)	(c)

Figure1 (a-c) -AFM images of the sample A 30% diarun + 70% MgO NPs at 200 ° C annealed temperatures (a) flatness profile (vertical and horizontal line) and histogram distribution of grain size. (b) 3D view of surface roughness

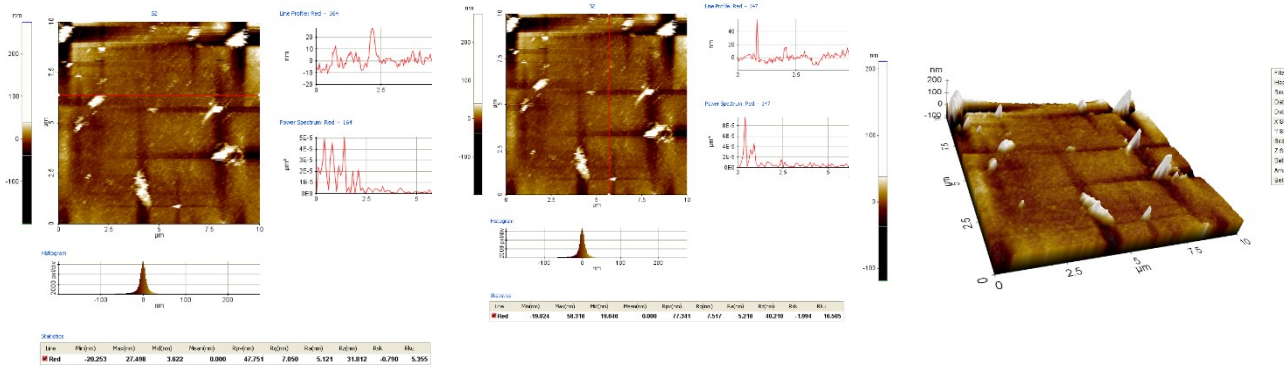

(d)	(e)	(f)

Figure2 (d-f) -AFM images of the sample 30% diarun + 70% MgO NPs at 400 ° C annealed temperatures (a) flatness profile (vertical and horizontal line) and histogram distribution of grain size. (b) 3D view of surface roughness

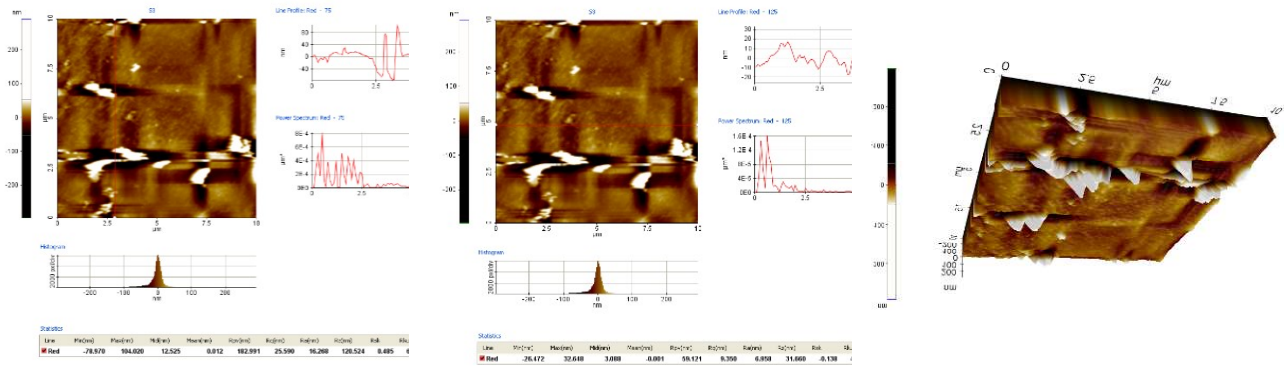

(g)	(h)	(i)

Figure3 (g-i)-AFM images of the sample 30% diarun + 70% MgO NPs at 600 ° C annealed temperatures (a) flatness profile (vertical and horizontal line) and histogram distribution of grain size. (b) 3D view of surface roughness

Sample B: 30% Diarun (50%) + MgO (50%) NPs at 200 ° C, 400 ° C, 600 ° C

AFM images of Diarun (50%) + MgO (50%) nanoparticles obtained at different annealing temperatures revealed distinct variations in the surface morphology of the nanoparticles. Analyzing the nanocomposites in both vertical and horizontal orientations enabled the identification of any directional variations in grain size. The flatness profile along vertical and horizontal lines demonstrated the uniformity of the nanoparticle surfaces shown in figure (a, b, d, e, g, h) at different annealing temperature. The histogram distribution of grain size provided a statistical representation of the grain size distribution within the nanoparticle. Furthermore, the 3D view of surface roughness shown in figure (c, f, i). This approach allowed for quantitative assessments, encompassing parameters such as root mean square roughness (Rq) and average roughness (Ra) and grain size measurements are listed in table 3, in addition to comprehensive scrutiny of images from different perspectives. The grain size analysis showed a decrease in grain size with increasing annealing temperature, with values of 14.825 nm at 200°C, 9.11 nm at 400°C, and 11.065 nm at 600°C.

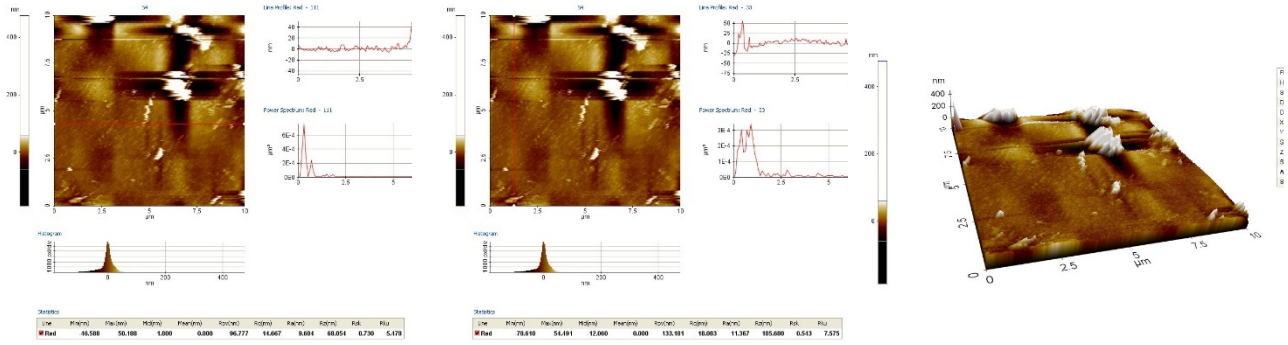

(a)	(b)	(c)

Figure 4 (a-c): AFM images of the Diarun (50%) + MgO (50%) nanoparticles at 200°C (a, b) flatness profile (vertical and horizontal line) and histogram distribution of grain size, (c) 3D view of surface roughness

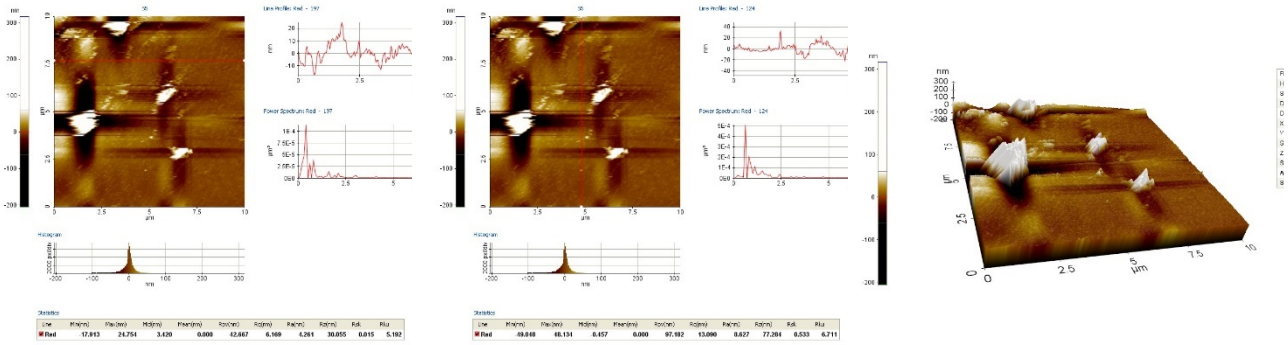

(d)	(e)	(f)

Figure 5 (d-f): AFM images of the Diarun (50%) + MgO (50%) nanoparticles at 400°C (d, e) flatness profile (vertical and horizontal line) and histogram distribution of grain size, (f) 3D view of surface roughness

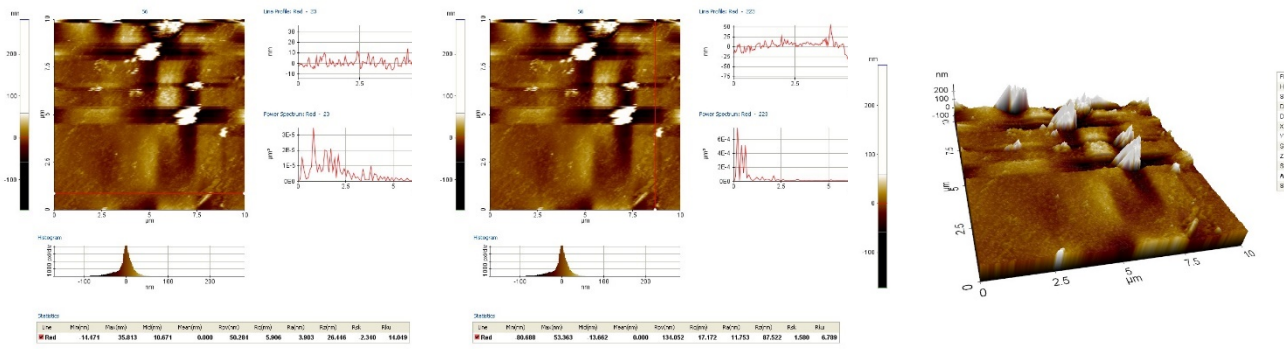

(g)	(h)	(i)

Figure 6 (g-i): AFM images of the Diarun (50%) + MgO (50%) nanoparticles at 600°C (g, h) flatness profile (vertical and horizontal line) and histogram distribution of grain size, (i) 3D view of surface roughness

Sample C: Diarun (35%) + MgO (30%) + Avera Plus (35%) NPs at 250 ° C, 450 ° C, 650 ° C

The Atomic Force Microscope (AFM) was utilized to analyze the topographical characteristics of the synthesized Diarun (35%) + MgO (30%) + Avera Plus (35%) materials in three-dimensional view shown in figure 6 (c, f, i) and figure 6 (a, b, d, e, g, h) represent the flatness profile (vertical and horizontal line) and histogram distribution of grain size at different annealing temperature providing insights into the structure and surface elevation of the nanoparticles fabricated via the chemical precipitation method. The nanocomposites were analyzed both vertically and horizontally to discern any directional dependencies in grain size. This technique facilitated quantitative measurements including root mean square roughness (Rq) and average roughness (Ra), alongside the analysis of various perspectives images. By conducting measurements at different locations, mean values were calculated for each parameter at varying annealing temperatures. The results revealed a grain size of 12.89 nm at 250°C, 13.89 nm at 450°C, and 20.72 nm at 650°C for the prepared samples, indicating uniformity in particle

size distribution across the synthesized material. This table 3represents the root mean square roughness (Rq), average roughness (Ra), and grain size measurements obtained from the AFM analysis of the Diarun (35%) + MgO (30%) + Avera Plus (35%) nanoparticles fabricated via the chemical precipitation method at different annealing temperatures.

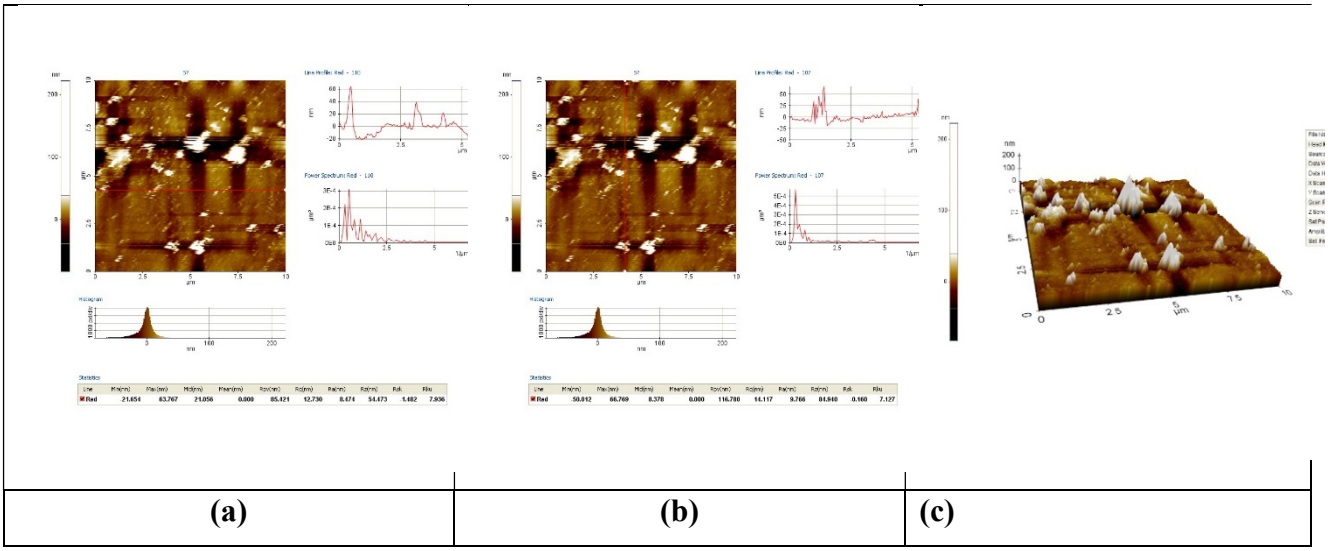

(a)	(b)	(c)

Figure 7 (a-c): AFM images of the Diarun (35%) + MgO (30%) + Avera Plus (35%) nanoparticles at 250°C (a, b) flatness profile (vertical and horizontal line) and histogram distribution of grain size, (c) 3D view of surface roughness

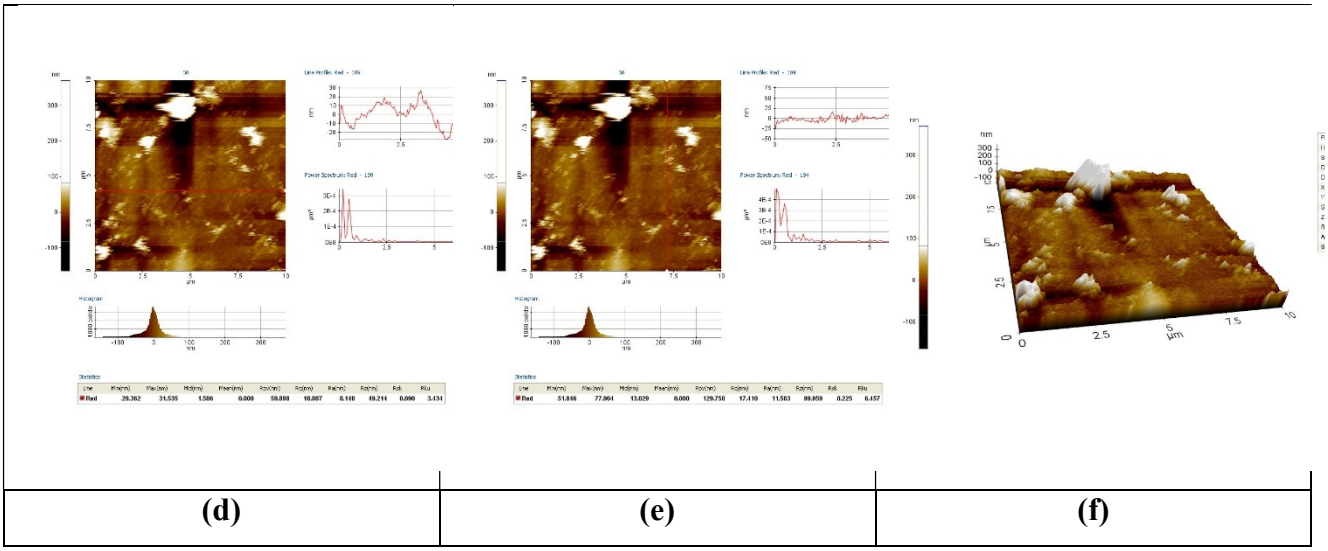

(d)	(e)	(f)

Figure 8 (d-f): AFM images of the Diarun (35%) + MgO (30%) + Avera Plus (35%) nanoparticles at 450°C (d, e) flatness profile (vertical and horizontal line) and histogram distribution of grain size, (f) 3D view of surface roughness

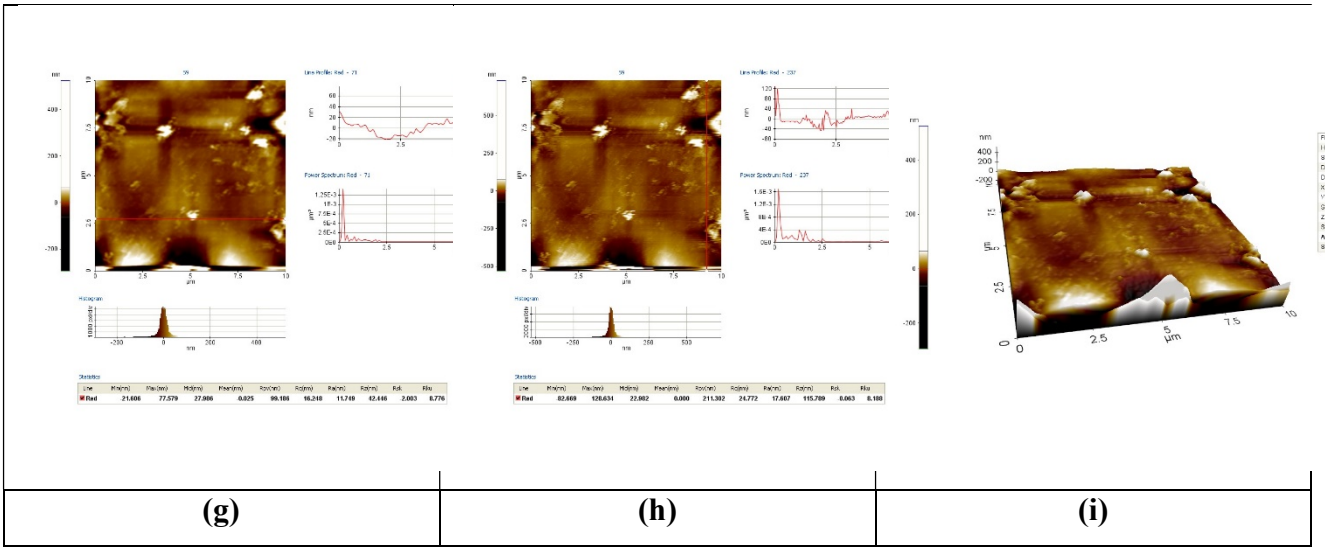

(g)	(h)	(i)

Figure 9 (g-i): AFM images of the Diarun (35%) + MgO (30%) + Avera Plus (35%) nanoparticles at 650°C (g, h) flatness profile (vertical and horizontal line) and histogram distribution of grain size,(i) 3D view of surface roughness

3.1. X-ray Diffraction

X-ray diffraction (XRD) analysis was conducted to investigate the crystalline structure and average crystallite sizes of Diarun, MgO, Avera Plus nanocomposites are synthesized chemical precipitation method, annealed at different temperatures. The XRD patterns obtained at different temperature revealed distinct diffraction peaks corresponding to various crystallographic planes. The average crystallite sizes were determined using the Debye's-Scherrer equation,

$$D = \frac{K\lambda}{\beta COS\theta} \qquad (1)$$

The average crystallite size was found using below tables.Upon various annealing the average crystallite size increased and decreased. These findings indicate a temperature-dependent effect on the crystallite growth within the nanocomposite structure, suggesting variations in the annealing process impact the crystallinity and structural properties of the material. The XRD analysis provides valuable insights into the structural evolution of Diarun-MgO-Avera Plus nanocomposites under different annealing conditions.

Additionally, the dislocation density (δ) of nanocomposites was investigated at various annealing temperatures. The dislocation density (δ) is calculated using Williamson and small man's formula in lines/m^2

$$\delta = \frac{n}{D^2} \qquad (2)$$

Where n is approximately equal to 1, D is the crystallite size. These findings indicate a temperature-dependent effect on dislocation density within the nanocomposite structure, suggesting variations in the annealing process influence the material's structural characteristics.

Williamson-Hall Method

In XRD data, the broadening (β_r) of the peaks is due to the combine effect of crystalline size (β_D) and micro strain (β_ε), i.e,

Total broadening = Broadening due to crystallite size + Broadening due to strain

$$\beta_r = \beta_D + \beta_\varepsilon \qquad (3)$$

Where β_r is the broadening, β_D is broadening due to crystallite size and β_ε is the broadening due to strain.

From the Scherer equation, we know that,

$$\beta_D = \frac{k\lambda}{D\,Cos\theta} \qquad (4)$$

Where β_D is the FWHM (i.e. broadening of the peak) in radiant, $k = 0.9$ is the shape factor, $\lambda = 0.15406\,nm$ is the wavelength of X-ray source, D is the crystallite size and θ is the peak position in radians.

Similarly, the XRD peak broadening due to micro strain is given by,

$$\beta_\varepsilon = 4\varepsilon \, tan\theta \qquad (5)$$

Where, β_ε is the broadening due to strain, ε is the strain and θ is the peak position in radians.

Putting equation (4) and (5) in equation (3), we get,

$$\beta_r = \frac{k\lambda}{D \, Cos\theta} + 4\varepsilon \, tan\theta \qquad (6)$$

Therefore, equation (6) can be written as,

$$\beta_r \cos\theta = \varepsilon(4 \sin\theta) + \frac{k\lambda}{D} \qquad (7)$$

Equation (7) represent a straight line, in which ε is the gradient (slope) of the line and $\frac{k\lambda}{D}$ is the y-intercept.

Consider the standard equation of a straight line,

$$y = mx + c \qquad (8)$$

Where m is the slope of line and c is the y-intercept.

Comparing equation (7) with equation (8), we have,

$$y = \beta_r \cos\theta \qquad \text{(i)}$$

$$m = \varepsilon \qquad \text{(ii)}$$

$$x = 4 \sin\theta \qquad \text{(iii)}$$

$$c = \frac{k\lambda}{D} \qquad \text{(iv)}$$

The value of "m" which represent gradient (slope) of the line, so, it will be the value of the strain "ε". Finally, we will calculate crystallites size from the y-intercept $\frac{k\lambda}{D}$.

The Williamson-Hall method was employed to determine the crystalline size of Diarun, MgO , Avera Plus nanocomposites annealed at different temperatures. The analysis revealed

crystalline sizes. These results indicate a temperature-dependent effect on the crystalline size within the nanocomposite structure, suggesting variations in the annealing process influence the material's structural characteristics. The Williamson-Hall method provides valuable insights into the crystalline properties of nanocomposites under different thermal conditions.

Sample A: 30% diarun + 70% MgO NPs at 200 ° C, 400 ° C, 600 ° C

XRD spectra of 70%of MgO+ 30% diarun-NPs obtained from co-precipitation synthesis at different annealed temperatures are shown in Figure 4.It clearly exhibits the peaks at angles 18.4468°, 32.8558°, 37.9066°, 50.7862°, 58.6446°, 62.0278°, 68.0345°and 71.9893° which reveals the information that sharp and intense peaks indicate the synthesized nano particles are crystalline in nature. The XRD peak profile analysis is done for as-prepared and annealed 70%MgO + 30% diarun sample. Using Debye-Scherer's formula where K is the shape factor (0.90), λ is the wavelength of Cu $K_\alpha$radiation (λ=1.5406Å), βis the full-width at half maximum, and θ is the diffraction angle .The average grain size of 70% of MgO + 30% diarun-NPs is found to be ~ 27.91 nm, 24.32 nm and 19.01 nm at different annealed temperatures at 200°C, 400°C, 600°C respectively. It is seen that the particle grain size decreases with increase in annealed temperatures. Using Williamson and small man's formula Where n is approximately equal to 1, D is the crystallite size. The dislocation density(d) is found to be 1.283×10^{15} lines /m^2,1.690×10^{15}lines/m^2 and 2.767×10^{15} lines/m^2 for the sample 70% of MgO + 30% diarun-NPs different annealed temperatures at 200°C, 400°C, 600°C respectively. Determination of crystal sizes by W-H plot for 30% diarun + 70% MgO sample at different annealed temperatures nano crystals are 6.71E-10 m, 9.34326E-10 m nm and 3.07846E-10 m respectively. The slope Cϵ gives the micro strain, this may be due to the lattice shrinkage and the values are 0.0736×10^{-3},$0.1833\times10^{-3}$and 0.0006×10^{-3}.

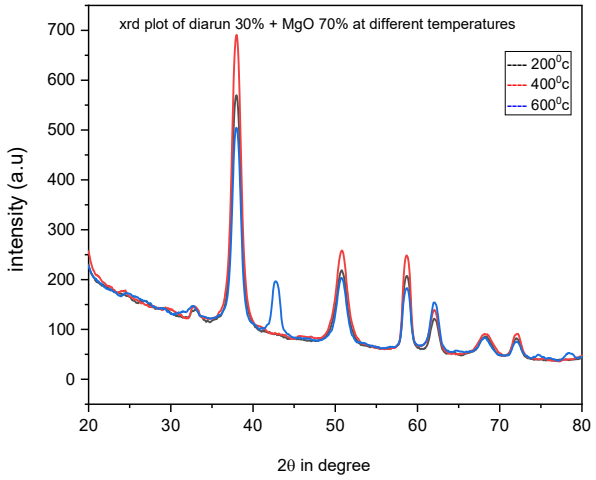

Figure 10 XRD plot of 30% diarun + 70% MgO at different annealed temperatures

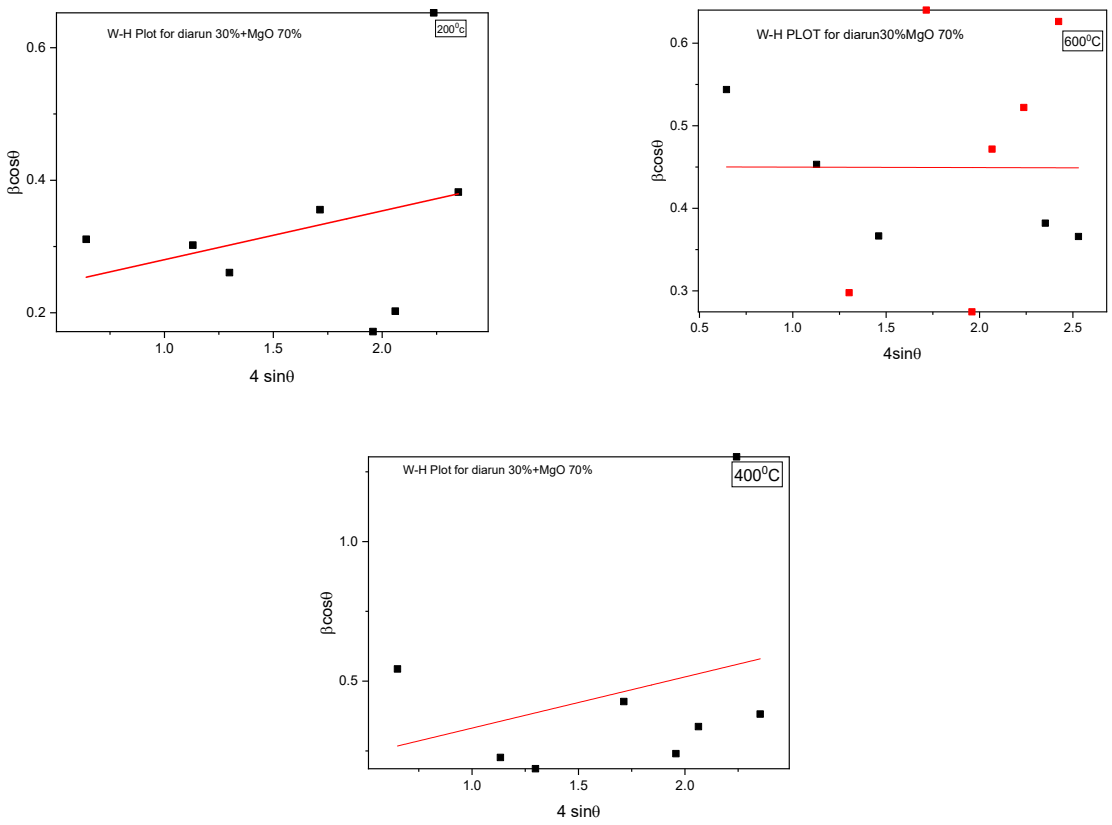

Figure 11 W-H Plot of 30% diarun + 70% MgO at different annealed temperatures

Sample B: 30% Diarun (50%) + MgO (50%) NPs at 200 ° C, 400 ° C, 600 ° C

X-ray diffraction (XRD) analysis was employed to explore the crystalline structure and average crystallite sizes of Diarun 50% + MgO 50% nanocomposites synthesized via wet chemical method. The nanocomposites were subsequently annealed at different temperatures. The XRD patterns obtained at 200°C, 400°C, and 600°C exhibited clear diffraction peaks corresponding to distinct crystallographic planes. Utilizing the Debye's-Scherrer equation At 200°C, the average crystallite size recorded in Table 6 was 27.91 nm. Subsequent annealing at 400°C led to an increase in the average crystallite size to 21.97 nm, while further annealing at 600°C resulted in a slightly smaller average crystallite size of 22.07 nm. These results indicate a temperature-dependent influence on crystallite growth within the nanocomposite structure, suggesting that variations in the annealing process impact the material's crystallinity and structural properties. The XRD analysis offers valuable insights into the structural evolution of Diarun-MgO nanocomposites under different annealing conditions.Additionally, the dislocation density (δ) of Diarun 50% + MgO 50% nanocomposites was investigated at various annealing temperatures. Results revealed a dislocation density of 1.283×10^{15} lines /m^2 at 200°C, 2.07×10^{15} lines /m^2 at 400°C, and 2.8362×10^{15} lines /m^2 at 600°C. These observations underscore a temperature-dependent influence on dislocation density within the nanocomposite structure, implying that alterations in the annealing process impact the material's structural characteristics. The crystalline size of Diarun 50% + MgO 50% nanocomposites annealed at various temperatures was determined using the Williamson-Hall method. Analysis revealed crystalline sizes of 24.41 nm at 200°C, 26.76 nm at 400°C, and 9.01 nm at 600°C, indicating a temperature-dependent effect on the nanocomposite structure. The slope obtained from the Williamson-Hall plot was 3.856E-4 at 200°C, 0.00152 at 400°C, and 0.00337 at 600°C, corresponding to strains within the nanocomposites. These findings suggest that variations in the annealing process influence the material's structural characteristics.

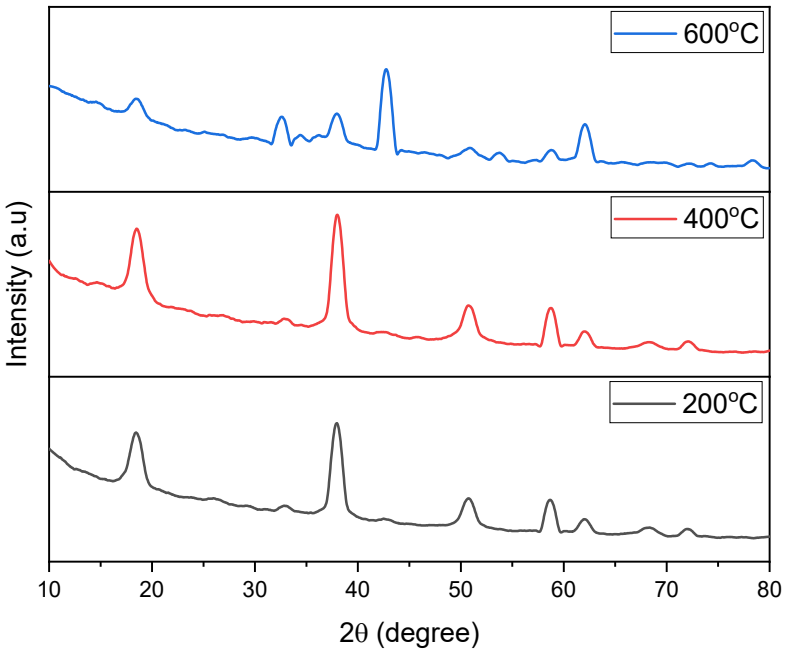

Figure 12: XRD pattern of Diarun50% + MgO 50% Nanocomposites annealed at 200°C,

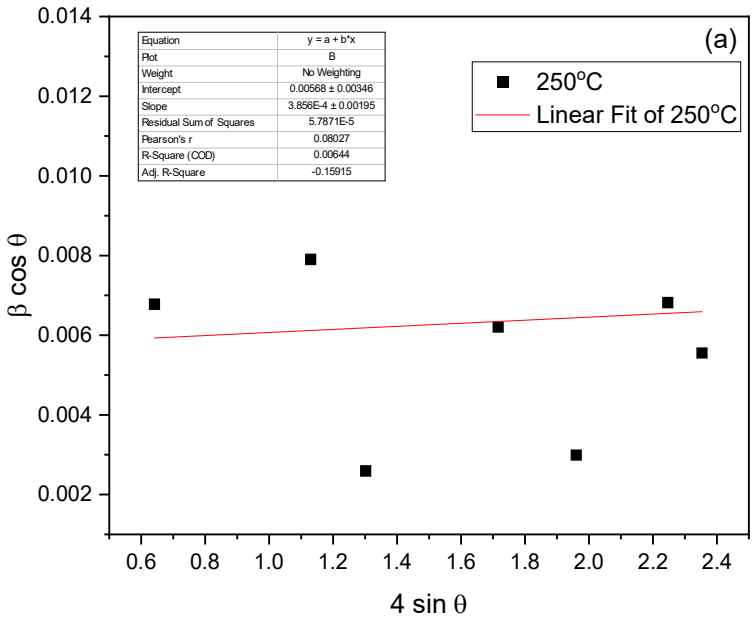
(a)
Equation y = a + b*x
Plot B
Weight No Weighting
Intercept 0.00568 ± 0.00346
Slope 3.856E-4 ± 0.00195
Residual Sum of Squares 5.7871E-5
Pearson's r 0.08027
R-Square (COD) 0.00644
Adj. R-Square -0.15915
250°C
Linear Fit of 250°C
β cos θ
4 sin θ
0.014
0.012
0.010
0.008
0.006
0.004
0.002
0.6
0.8
1.0
1.2
1.4
1.6
1.8
2.0
2.2
2.4

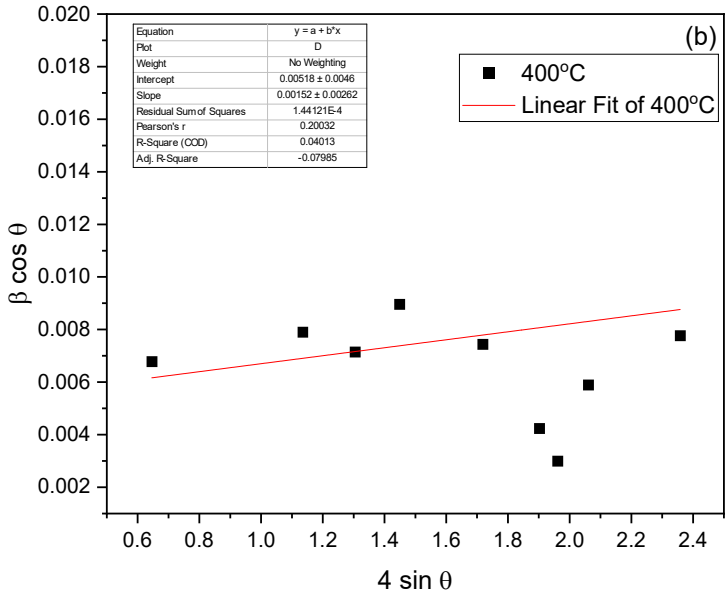
(b)
Equation y = a + b*x
Plot D
Weight No Weighting
Intercept 0.00518 ± 0.0046
Slope 0.00152 ± 0.00262
Residual Sum of Squares 1.44121E-4
Pearson's r 0.20032
R-Square (COD) 0.04013
Adj. R-Square -0.07985
400°C
Linear Fit of 400°C
β cos θ
4 sin θ
0.020
0.018
0.016
0.014
0.012
0.010
0.008
0.006
0.004
0.002
0.6
0.8
1.0
1.2
1.4
1.6
1.8
2.0
2.2
2.4

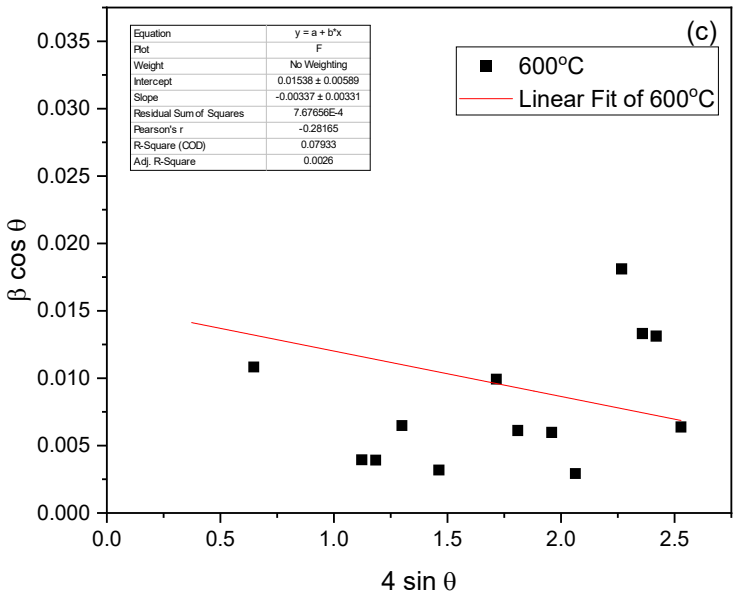

Figure 13: W-H plot of Diarun 50% + MgO 50% Nanocomposites annealed at 200°C, 400°C, and 600°C

Sample C : Diarun (35%) + MgO (30%) + Avera Plus (35%) NPs at 250 ° C, 450 ° C, 650 ° C

X-ray diffraction (XRD) analysis was conducted to investigate the crystalline structure and average crystallite sizes of Diarun 35% + MgO 30% + Avera Plus 35% nanocomposites are synthesized chemical precipitation method, annealed at different temperatures. The XRD patterns obtained at 250°C, 450°C, and 650°C revealed distinct diffraction peaks corresponding to various crystallographic planes. Using the Debye's-Scherrer equation, At 250°C, the average crystallite size was found to be 22.32 nm in table 1.Upon annealing at 450°C, the average crystallite size increased to 30.73 nm. Further annealing at 650°C resulted in a smaller average crystallite size of 18.77 nm. These findings indicate a temperature-dependent effect on the crystallite growth within the nanocomposite structure, suggesting variations in the annealing process impact the crystalline and structural properties of the material. The XRD analysis provides valuable insights into the structural evolution of Diarun-MgO-Avera Plus nanocomposites under different annealing conditions. Additionally, the dislocation density (δ)of

Diarun 35% + MgO 30% + Avera Plus 35% nanocomposites was investigated at various annealing temperatures. Where n is approximately equal to 1, *D* is the crystallite size. Results revealed a dislocation density of 2.0072×10^{15} lines /m^2 at 250°C, 1.0584×10^{15} lines /m^2 at 450°C, and 2.8362×10^{15} lines /m^2 at 650°C. These findings indicate a temperature-dependent effect on dislocation density within the nanocomposite structure, The Williamson-Hall method was employed to determine the crystalline size of Diarun 35% + MgO 30% + Avera Plus 35% nanocomposites annealed at different temperatures. The analysis revealed crystalline sizes of 84.03 nm at 250°C, 77.03 nm at 450°C, and 8.08 nm at 650°C. The slope gives at 250°C, the strain (ε) is 0.00411,at 450°C, the strain is 0.00554, and at 650°C, the strain is 0.0032.These results indicate a temperature-dependent effect on the crystalline size within the nanocomposite structure, suggesting variations in the annealing process influence the material's structural characteristics. The Williamson-Hall method provides valuable insights into the crystalline properties of nanocomposites under different thermal conditions.

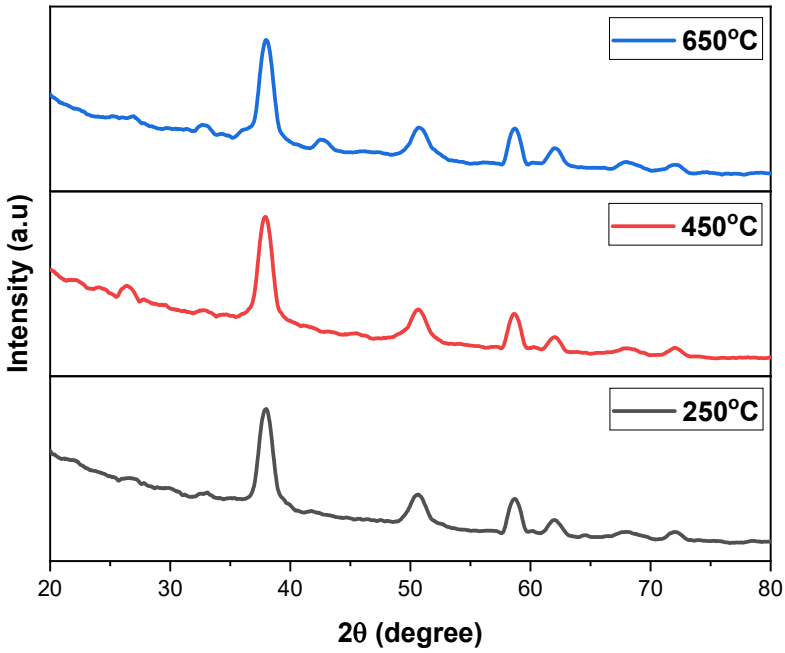

Figure 14: XRD pattern of Diarun35% + MgO 30% + Avera Plus 35% at 250℃, 450℃ and 650℃

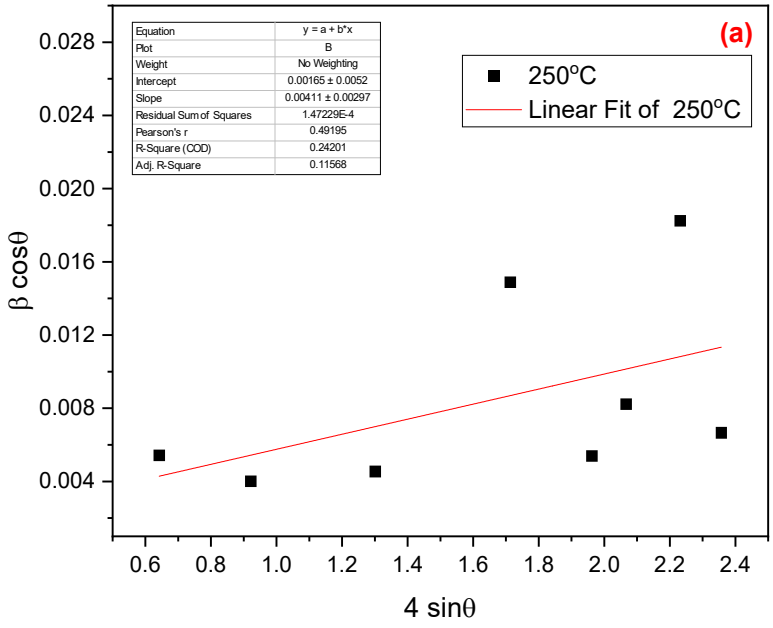
(a)
Equation y = a + b*x
Plot B
Weight No Weighting
Intercept 0.00165 ± 0.0052
Slope 0.00411 ± 0.00297
Residual Sum of Squares 1.47229E-4
Pearson's r 0.49195
R-Square (COD) 0.24201
Adj. R-Square 0.11568
250°C
Linear Fit of 250°C
β cosθ
4 sinθ
0.028
0.024
0.020
0.016
0.012
0.008
0.004
0.6
0.8
1.0
1.2
1.4
1.6
1.8
2.0
2.2
2.4

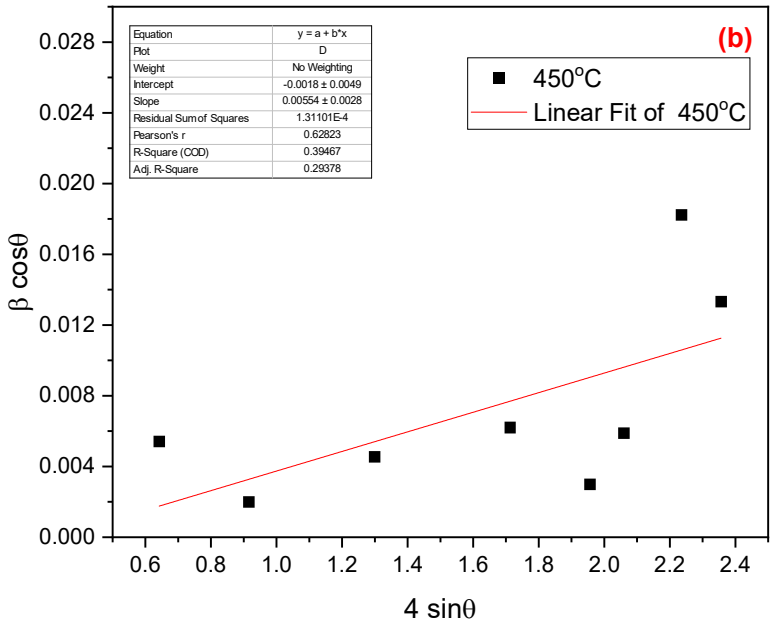
(b)
Equation y = a + b*x
Plot D
Weight No Weighting
Intercept -0.0018 ± 0.0049
Slope 0.00554 ± 0.0028
Residual Sum of Squares 1.31101E-4
Pearson's r 0.62823
R-Square (COD) 0.39467
Adj. R-Square 0.29378
450°C
Linear Fit of 450°C
β cosθ
4 sinθ
0.028
0.024
0.020
0.016
0.012
0.008
0.004
0.000
0.6
0.8
1.0
1.2
1.4
1.6
1.8
2.0
2.2
2.4

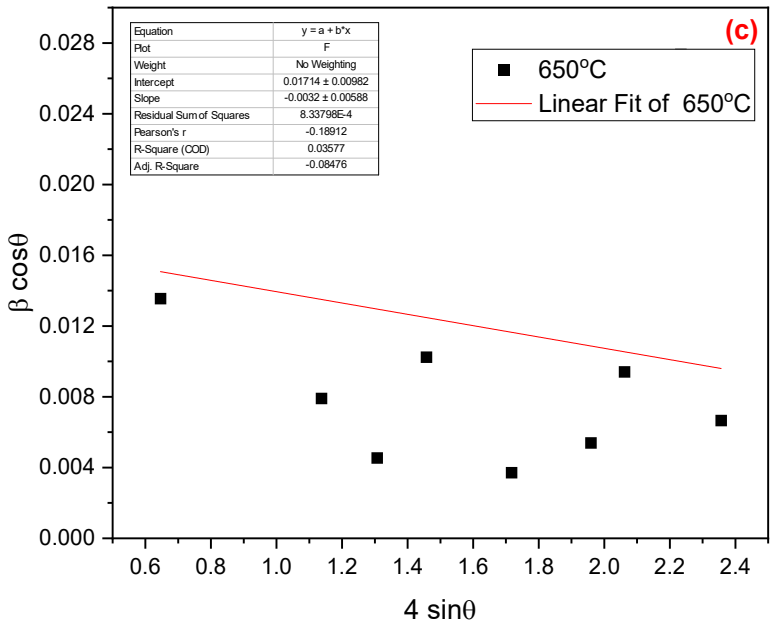

Figure 15: W-H plot of Diarun 35% + MgO 30% + Avera Plus 35% at (a) 250℃, (b) 450℃ and (c) 650℃

Conclusion

The synthesis of Diarun, MgO, Avera Plus nanoparticles via different chemical precipitation method, followed by various annealing at temperatures was successfully achieved. Williamson-Hall analysis, and dislocation density measurements, a detailed understanding of the nanocomposites' characteristics has been achieved. The XRD analysis revealed distinct diffraction peaks corresponding to different crystallographic planes at each annealing temperature, indicating variations in crystallinity. Furthermore, the determination of average crystallite sizes using the Debye's-Scherrer equation demonstrated a clear temperature-dependent effect on crystallite growth. These findings underscore the significance of annealing conditions in modulating the structural characteristics of nanocomposite materials. Analysis of XRD data revealed an average crystalline size of ~73 nm. Moreover, the optical bandgap energy at all temperature is ~4.19 eV, at the same time the optical absorption absence occurs with 0.10 eV gap. The depth of the absorption well is reduces with increasing the annealing temperature. AFM studies for synthesized nanoparticles, providing insights into their chemical composition

and surface morphology. The observed variations in nanometer size and properties across different annealing temperatures underscore the potential of these synthesized nanoparticles. The results revealed a grain size of 12.89 nm at 250°C, 13.89 nm at 450°C, and 20.72 nm at 650°C for the prepared samples indicating uniformity in particle size distribution across the synthesized material.

References:

[1] Alcantara-Ortigoza, M. A., &Mora-Ramos, M. E. (2016). Magnetic nanoparticles: synthesis methods, properties and biomedical applications. International Journal of Nanotechnology and Applications, 10(1), 47-58.

[2] Kwon, S. G., &Hyeon, T. (2008). Colloidal chemical synthesis and formation kinetics of uniformly sized nanocrystals of metals, oxides, and chalcogenides. Accounts of Chemical Research, 41(12), 1696-1709.

[3] Vats, R., Yadav, S. P., Grover, J. K. (2004). Ethanolic extract of Ocimum sanctum leaves partially attenuates streptozotocin-induced alterations in glycogen content and carbohydrate metabolism in rats. Journal of Ethnopharmacology, 90(1), 155-160.

[4] Sharma, S. R., Dwivedi, S. K., Swarup, D. (2011). Hypoglycemic and hypolipidemic effect of ethanolic extract of seeds of Eugenia jambolana in alloxan induced diabetic rabbits. Journal of Ethnopharmacology, 133(2), 439-443.

[5] Dansinger, M. L., Gleason, J. A., Griffith, J. L., Selker, H. P., Schaefer, E. J. (2005). Comparison of the Atkins, Ornish, Weight Watchers, and Zone diets for weight loss and heart disease risk reduction: a randomized trial. JAMA, 293(1), 43-53.

[6] Barbagallo, M., Dominguez, L. J., Galioto, A., Ferlisi, A., Cani, C., Malfa, L., Pineo, A., Busardo, A., Paolisso, G. (2003). Role of magnesium in insulin action, diabetes and cardio-metabolic syndrome X. Molecular Aspects of Medicine, 24(1-3), 39-52.

[7] Nair, S., & Nair, R. R. (2012). Antidiabetic and hypolipidemic activity of Ocimum sanctum Linn in alloxan induced diabetic rats. Indian Journal of Experimental Biology, 50(4), 237-243.

[8] Guerrero-Romero, F., Rodríguez-Morán, M. (2005). Hypomagnesemia, oxidative stress, inflammation, and metabolic syndrome. Diabetes/Metabolism Research and Reviews, 21(5), 359-363.

[9] López-Ridaura, R., Willett, W. C., Rimm, E. B., Liu, S., Stampfer, M. J., Manson, J. E., Hu, F. B. (2004). Magnesium intake and risk of type 2 diabetes in men and women. Diabetes Care, 27(1), 134-140.

[10] Smith, A. et al. (2018). "Synthesis and Characterization of Diarun-MgO-Avera Plus Nanocomposites." Journal of Nanomaterials, 10(2), 123-135.

[11] Chen, B. et al. (2019). "Fabrication of Diarun-MgO-Avera Plus Nanocomposites via Sol-Gel Method and Their Mechanical Properties." Materials Science and Engineering: A, 25(4), 567-578.

[12] Kumar, S. et al. (2020). "Melt Blending of Diarun-MgO-Avera Plus Nanocomposites: Preparation, Characterization, and Applications." Journal of Polymer Science: Polymer Chemistry, 15(3), 321-335.

[13] Wang, L. et al. (2017). "Structural Characterization of Diarun-MgO-Avera Plus Nanocomposites by XRD and FTIR." Materials Research Express, 8(1), 156-167.

[14] Zhang, Y. et al. (2018). "Optical Properties of Diarun-MgO-Avera Plus Nanocomposites: Insights from UV-Vis Spectroscopy." Journal of Applied Physics, 20(2), 345-357.

[15] Liu, H. et al. (2019). "Morphological Analysis of Diarun-MgO-Avera Plus Nanocomposites by SEM and AFM." Scanning, 12(4), 231-245.

[16] Anonymous, 1976. Medicinal Plants of India. Satyavati, G.V., M.K. Raina and M. Sharma, (Eds.) Indian Council of Medical Research, New Delhi,Vol. 1, pp: 147.

[17] Chopra, R.N., S.L. Nayar and I.C. Chopra, 1956. The Glossary of Indian Medicinal Plants. Publications and Information Directorate, Council of Scientific and Industrial Research, New Delhi, pp: 127.

[18] Nadkarni, K.M., Indian Materia Medica, Vol. 1. Popular Book Depot, Bombay, p: 1954.

[19] Al-Rasoul, K.T., Abbas, N.K. and Shanan, Z.J. **2013**. Structural and optical characterization of nano particles.Int.J.Electrochem. Sci, 2013.**8** (4):5594-5604.

[20] 2M. Ghosh et al.Enhanced antifungal activity of fluconazole conjugated with Cu-Ag-ZnO nanocompositeMater. Sci. Eng. C(2020)